New perspectives in Plasticity theory: dislocation nucleation, waves, and partial continuity of plastic strain rate

Amit Acharya[1], Armand Beaudoin[2], Ron Miller[3]
[1]Carnegie Mellon University, USA, [2] University of Illinois at Urbana-Champaign, USA,
[3]Carleton University, Canada

Abstract

A field theory of dislocation mechanics and plasticity is illustrated through new results at the nano, meso, and macro scales. Specifically, dislocation nucleation, the occurrence of wave-type response in quasi-static plasticity, and a jump condition at material interfaces and its implications for analysis of deformation localization are discussed.

1. Introduction

We review a PDE model of plasticity (Acharya 2004; Acharya and Roy, 2006) that allows a discussion of mechanical response at different scales, as it arises from the stress field and motion of dislocations in an elastic solid. At the nanoscale, the model makes a prediction for a driving force for dislocation nucleation and the associated slip (Acharya, 2003, 2004; Miller and Acharya, 2004). In this paper, we physically interpret this prediction. On elementary space-time averaging of this nanoscale nonlinear system, a mesoscale system of PDE emerges that makes a connection between classical plasticity modeling and the elastic theory of continuously distributed dislocations. A primary conceptual modification of this theoretical setup over conventional plasticity is a clear kinematical definition of *excess* (or geometrically-necessary-dislocation GND) and *statistical* dislocation (statistically-stored-dislocation SSD) densities related to the scale of observation, and an allowance for the motion of both as contributing to the total plastic strain rate. This feature turns the evolution equation for the excess dislocation density into a nonlinear transport equation displaying features of wave propagation that needs to be solved as a primary field equation, in sharp contrast to being a 'passively' determined field obtained by taking the curl of a constitutively specified plastic strain rate. More importantly, this formulation as a field equation implies jump conditions of physical relevance at surfaces of discontinuity (Acharya, 2007). Taken together, these features allow for a stabilizing effect in situations corresponding to softening plasticity, the prediction of moving plastic fronts, and *size-independent* nonlocal effects in macroscopic plasticity in the presence of inhomogeneous plastic deformation. In this paper, we discuss and illustrate each of these features (of course, size-dependent nonlocal effects are also predicted by the theory). To state a facile analogy with fluid turbulence modeling, the classical constitutive specification of plastic strain rate emerges as a subgrid term in the new theoretical structure; the modifications that this structure imposes on conventional plasticity amounts to defining the governing equations for the dynamics of the 'large eddies' (excess dislocation density) and their coupling to the energetics and dynamics of the 'smaller' ones (statistical dislocation density).

Detailed connections of our theory with work in the literature, both classical as well as recent, can be found in (Acharya, 2001; Roy and Acharya, 2005; Acharya and Roy, 2006). A series of

works by Limkumnerd and Sethna (2006a, 2007, 2006b) that have since appeared is based on essentially the same theory as recognized by the authors (Limkumnerd and Sethna, 2006b). Motivated by their numerical results, these authors suggest that the theory admits singularities in the Nye tensor field even when the elastic response is linear, an interesting claim that would be well worth establishing rigorously. The characterization of stress-free states is dealt with in a Fourier-transform setting with its associated limitations in Limkumnerd and Sethna (2007); of course, stress free states of continuum distributions of dislocations can be dealt with in the greater generality of a real-space setting of finite bodies, as can be deduced from the works of Kröner (1981) and Mura (1989), as shown in Head et al. (1993) and Acharya (2003).

This paper is organized as follows: in Section 2 we discuss the phenomena of dislocation nucleation and motion, as manifested in atomistic simulations. The discussion illuminates the difference between the physical meanings of dislocation nucleation and motion. In Section 3, the theory of Field Dislocation Mechanics (FDM) and its averaged counterpart, Mesoscopic Field Dislocation Mechanics (MFDM) are briefly described. In Section 4, the driving forces for dislocation nucleation and the associated slip in FDM are interpreted physically, leading to partial guidance on a criterion for dislocation nucleation. In Section 5, a finite element implementation of PMFDM (Phenomenological MFDM), i.e. MFDM augmented with phenomenological constitutive assumptions, is used to model the propagation of a plastic front in a whisker as observed in experiment. This propagation is triggered by the sudden motion of subgrid, statistical, mobile dislocations leading to a temporary stress softening response, and it is shown to be catastrophic in conventional, rate-dependent, plasticity theory which is incapable of predicting such propagation. Finally, in Section 6 we consider the partial continuity conditions on plastic strain rate implied by the theory on a surface of discontinuity not moving with respect to the material. The theory suggests that such a condition should apply even in conventional plasticity theory. Conventionally, the evolution equation for the plastic deformation in standard local plasticity is an ordinary differential equation and therefore can be entirely discontinuous in space, e.g. at a static grain boundary. Thus, the new jump condition implies a size-independent nonlocal feature in heterogeneous conventional plasticity and an implication with respect to conditions for strain localization is discussed.

2. Dislocation nucleation and motion in atomistic simulation

Considering dislocations as the only lattice defects for simplicity, slip or permanent deformation in a crystal is produced by the mechanisms of dislocation motion and nucleation. The essential physical difference between these two types of slip is that nucleation of a dislocation involves the instantaneous slip of many atoms in a slip plane whereas motion of a dislocation over a time interval comparable to that required for nucleation involves the slip of only a few atoms on the slip plane. An idealized picture of these two phenomena is schematically described in Fig. 1.

The physical differences between the mechanisms of dislocation nucleation and dislocation motion can be readily understood through atomistic simulations. Here, we focus our attention on dislocation nucleation and subsequent motion beneath a surface indented by a spherical indenter. What follows in this section is a summary of part of a recent paper by Miller and Rodney (2007), in which more detail can be found. Here in this review, we use the results of Miller and Rodney to better understand the details of the nucleation mechanism itself.

Using static (zero temperature) molecular statics within an embedded atom method (EAM) atomistic framework, Miller and Rodney pressed a rigid, frictionless sphere into an initially

perfect single crystal in both 2D and 3D. The 2D results are useful for visualization and understanding of the mechanism, and so we confine our attention here to these simpler results.

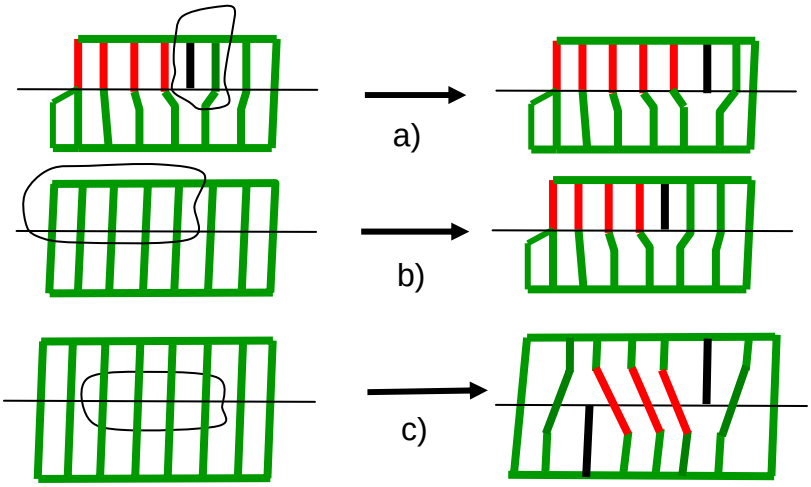

Figure 1. Schematic illustration of dislocation motion and nucleation; a) motion of an existing edge dislocation resulting in an advance of the slipped region; b) nucleation of an edge dislocation; c) nucleation of an edge dislocation dipole. Red lines indicate slipped regions of the crystal; green lines represent unslipped (but possibly deformed) regions; and black lines represent dislocations as the boundary between slipped and unslipped regions.

Miller and Rodney used a simple triangular lattice of atoms, interacting with the Ercolessi-Adams EAM potentials (Ercolessi and Adams (1994)) The lattice had a near-neighbor distance of a_0=2.83Å. The indenter was idealized as a perfect sphere using a repulsive indenter potential, along the lines of other authors (Kelchner et al. (1998), Knap and Ortiz (2001), Li et al. (2002), Miller et al. (2003), Miller and Acharya (2004)). Unless otherwise noted below, the indenter radius was R=100 A.

2.1 The Mechanisms of Homogeneous Nucleation

The model used for indentation along the [01] direction in the triangular lattice is shown in Fig. 2. Miller and Rodney studied this case using the static quasicontinuum (QC) method (Shenoy et al. (1999), Tadmor and Miller (2007)). The region beneath the indenter, extending approximately from -130 to 130 Å horizontally and from -120 to 0 Å vertically was fully atomistic. The inset on the top right of the figure shows the details of the lattice beneath the indenter.

In order to capture the first nucleation of a defect, it is necessary to take very small load steps as we approach the critical indenter penetration. To do this, Miller and Rodney used an algorithm whereby a given load step, Δd, was chosen and repeated until a defect nucleates. At this point, the last relaxed configuration *prior to* nucleation was restored, the size of the load step reduced by a factor of two, and the process repeated until the load step size was below some tolerance. In this way, it is possible to capture the configuration of the atoms so close to nucleation that subsequent indenter motion of less that $1\text{x}10^{-6}$ Å triggers nucleation, implying

that the final elastic configuration is, for all practical purposes, *right at* the point of instability leading to the first defect nucleation.
In Fig. 3, we show the region under the indenter just before and just after nucleation. A mesh is shown between the atoms, rather than the atoms themselves, to better appreciate the plastic deformation. The sheared elements indicate the plane along which slip has taken place, leaving a dislocation near the surface at the left edge of the indenter and another out of view towards the lower right side. The unstable nature of the nucleation process, coupled with the low Peierls barrier, means that the dislocations travel a long way from their initial nucleation site. In other words, it is difficult to isolate the actual *nucleation process* from the subsequent dislocation motion by which it is typically accompanied. To see the details of the nucleation itself and its

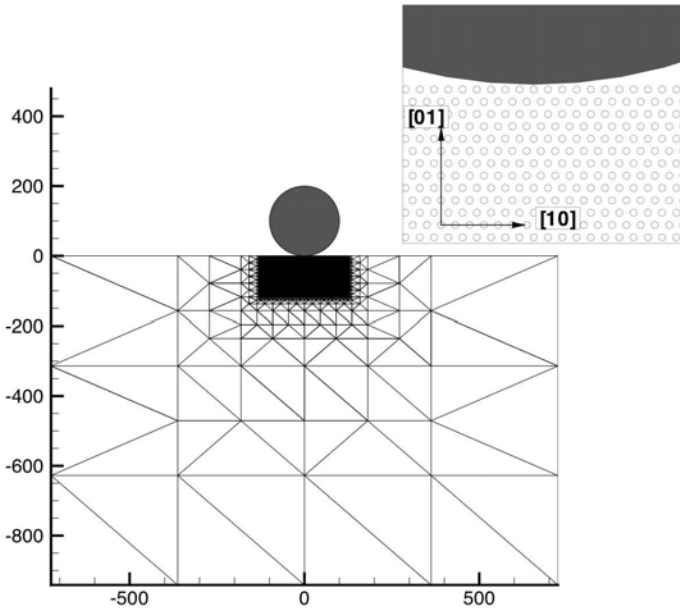

Figure 2: Indentation into a 2D triangular lattice along the [01] direction**. (After Miller and Rodney (2007).)**

exact location, it is necessary to look at intermediate configurations *during* the CG minimization between relaxed configurations (a) and (b) in figure Fig. 3, *i.e.*, at each configuration after a line minimization step.

Fig. 3 reveals the exact moment of dislocation nucleation by comparing the CG minimization steps just before and after the defect forms. We can see that the nucleation event is the instantaneous appearance of a dislocation dipole of finite size, corresponding to the collective motion of about 10 atoms on either side of the slip plane. One row of 10 atoms moves about 0.6 Å along the slip direction, while the next row moves about the same distance in the other direction. Other than these 20 or so atoms, there is very little movement. The value of 0.6 Å corresponds to about 1/4 of the Burgers vector, so that the total slip in the region is about b/2. After the formation of this ``nucleus", the formation of the full defect proceeds in two more steps as shown in Fig. 4. First, the Burgers vector of the dipole grows to reach the full b. Within about 10 minimization steps, the dislocation is fully formed and the dipole spacing has grown only slightly, to about 13 atomic spacings. Only then does the final step take place, during which

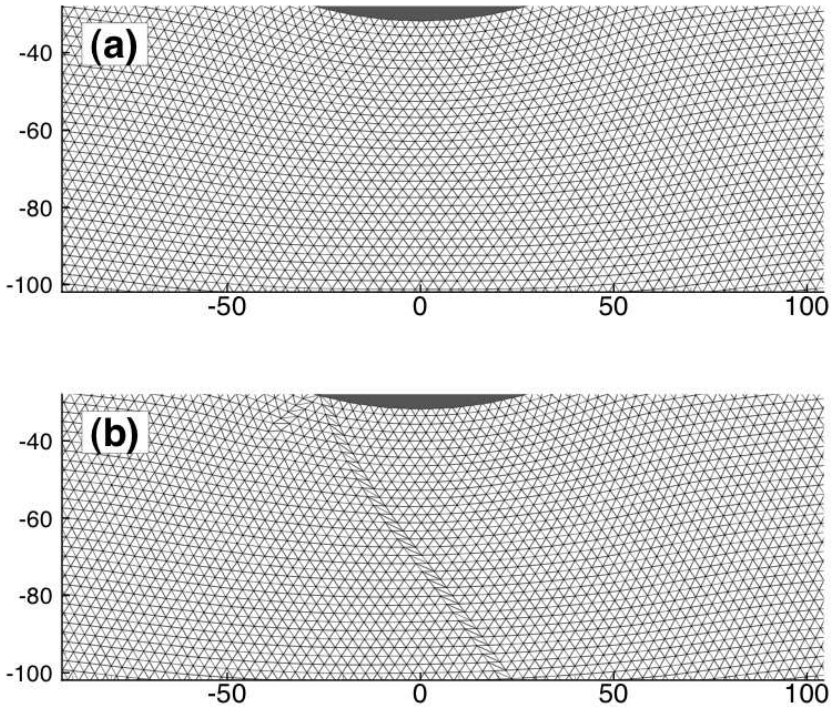

Figure 3: Configurations (a) just before and (b) just after dislocation nucleation during indentation into a 2D triangular lattice along the [01] direction. **(After Miller and Rodney (2007).)**

the fully formed dipole moves apart. However, although the final configuration involves two fully formed dislocations with a large separation between them, the true *nucleus* of plasticity is a dipole with about half the full Burgers vector.

Miller and Rodney have determined that this nucleation process is a signature of the indentation simulations, regardless of the crystal orientation, indenter size or model dimensionality (although of course the load level and precise location of the initial defect change). The size of this dipole is more or less constant with respect to the orientation of the crystal, *but grows with the size of the indenter*, an interesting point that we will return to right away.

In 3D, this process becomes the spontaneous formation of a loop, again of a finite size depending only on the size of the indenter. Miller and Rodney referred to the diameter of this critical nucleating disk (or dipole in 2D) as the ``nucleation diameter", d_{nuc}.

Qualitative snapshots of the 3D nucleation process, painting the general picture of how and where the initial defects form, are abundant in the literature (Kelchner et al. (1998), van Vliet et al. (2002), Knap and Ortiz (2003), van Vliet et al. (2003), Li (2007), Miller and Rodney (2007)), where the interested reader may find more detail.

Miller and Rodney studied the dependence of the nucleation diameter d_{nuc} on the indenter radius R, and found an approximately linear relationship between the indenter radius and the nucleation diameter, of a range of indenters from R=20 Å to R=2000 Å. This linear dependence leads to an interesting *size independence* of the ``hardness" associated with the first nucleation

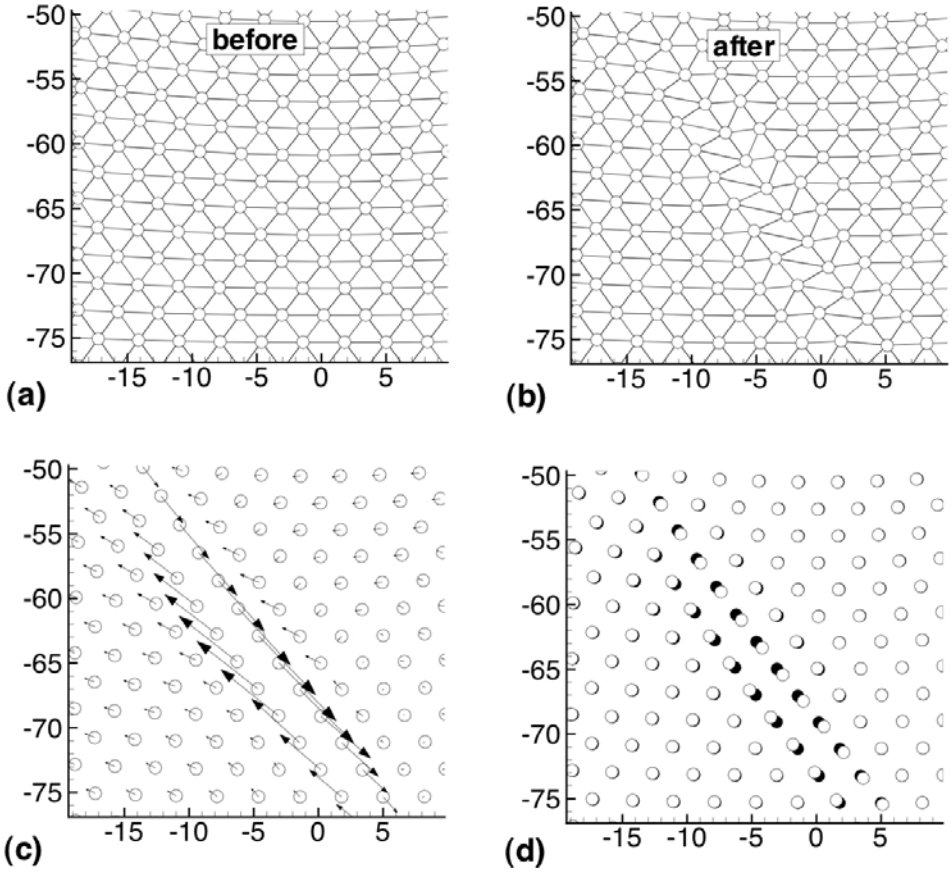

Figure 4 : Conjugate gradient minimization steps (a) just before and (b) Conjugate gradient minimization steps (a) just before and (b) just after nucleation. Vectors in (c) show the displacements of each atom during the minimization step magnified by a factor of 10, while (d) superimposes the atomic positions from (a) (shown in black) beneath those from (b) (shown in white). **(After Miller and Rodney 2007)**

event. Taking the hardness as the force on the indenter divided by the contact area (contact length in 2D) just prior to nucleation, Miller and Rodney demonstated that the nucleation hardness is virtually independent of the indenter size. By way of contrast, we note that nanoindentation experiments typically show a relatively strong size dependence of the inverse square root form (Nix and Gao (1998), Gerberich et al. (2002)). As such, this suggests that most plastic flow in experiments is governed by mechanisms other than homogeneous nucleation. Since the critical disk grows with the indenter size, we expect that homogeneous nucleation would rapidly become highly unlikely as the indenter size increases. This is because the probability of such a large region of crystal being free of any defects (including vacancies) becomes very small. On the other hand, for very small indenters, homogeneous nucleation may in fact occur.

Having gained an understanding of the physical mechanisms of nucleation, it is now worthwhile to summarize briefly the most significant points. The mechanism we have just described suggests a strongly *nonlocal* character, as nucleation is clearly a collective motion of

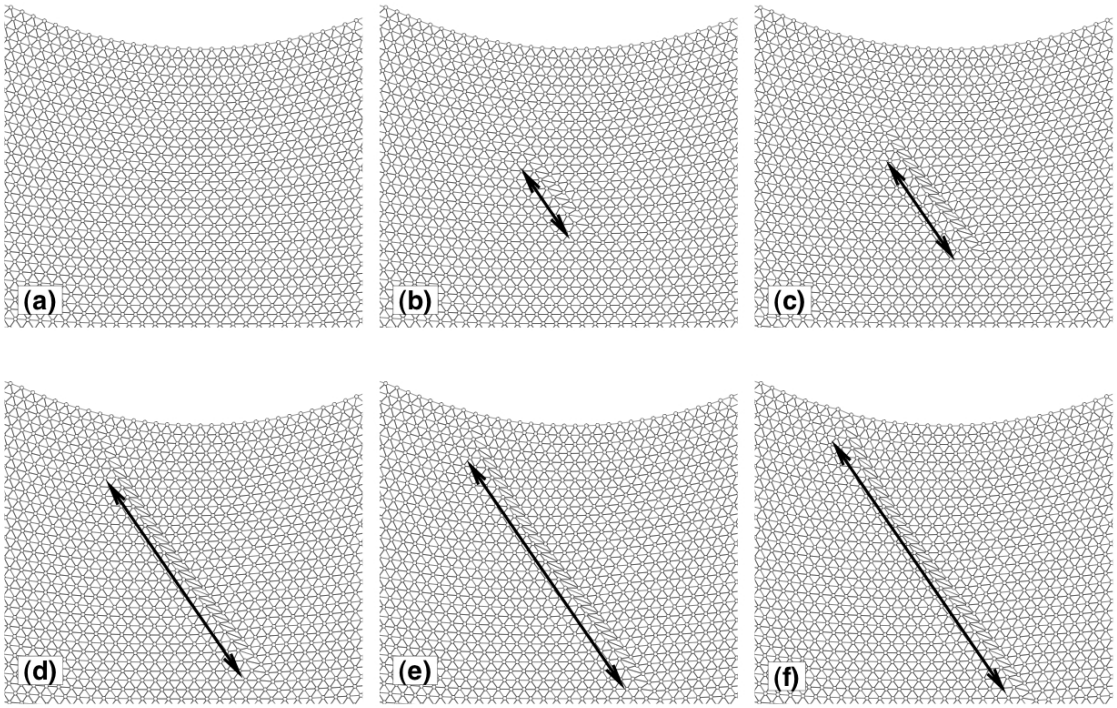

Figure 5: Nucleation and motion of a dislocation dipole during nano-indentation. (a) the undefected cystal. (b) nucleation (c) growth to a full Burgers vector and (d)-(f) motion.

several atoms over the slip plane and does not initiate at an isolated atomic position. Further, the fact that the nucleated disk grows with the indenter size points to a nucleation process that is in some sense sampling the *gradients* of the mechanical field variables (like stress). This highlights the need, within any theory, to include nonlocal effects, or at the least gradient effects, if we hope to have a reliable criterion for the nucleation process. Likewise, atomic-scale nucleation criteria based on an atom-by-atom quantity (such as, for example, the atomic level stress at an atom) are likely to be unable to accurately describe this process. A full discussion of these challenges and further examination of nucleation criteria is presented in Miller and Rodney (2007).

The effect of temperature on this process has not been addressed here. Certainly we expect, at least for low to moderate temperatures, that transition state theory will apply and the nucleation process becomes a stochastic one related to the size of energy barriers. Evidence that the nucleation mechanism is more or less unchanged at moderate temperatures was provided by Dupuy et al. (2005). There, simulations analogous to these were performed at finite temperature to reveal essentially the same nucleation mechanisms (albeit on a different crystal structure).

2.3 The Mechanisms of Dislocation Motion

The same 2D simulations of Miller and Rodney can be used to understand the mechanisms of dislocation motion by examining the atomistic configurations during CG minimization step subsequent to the initial defect nucleation.

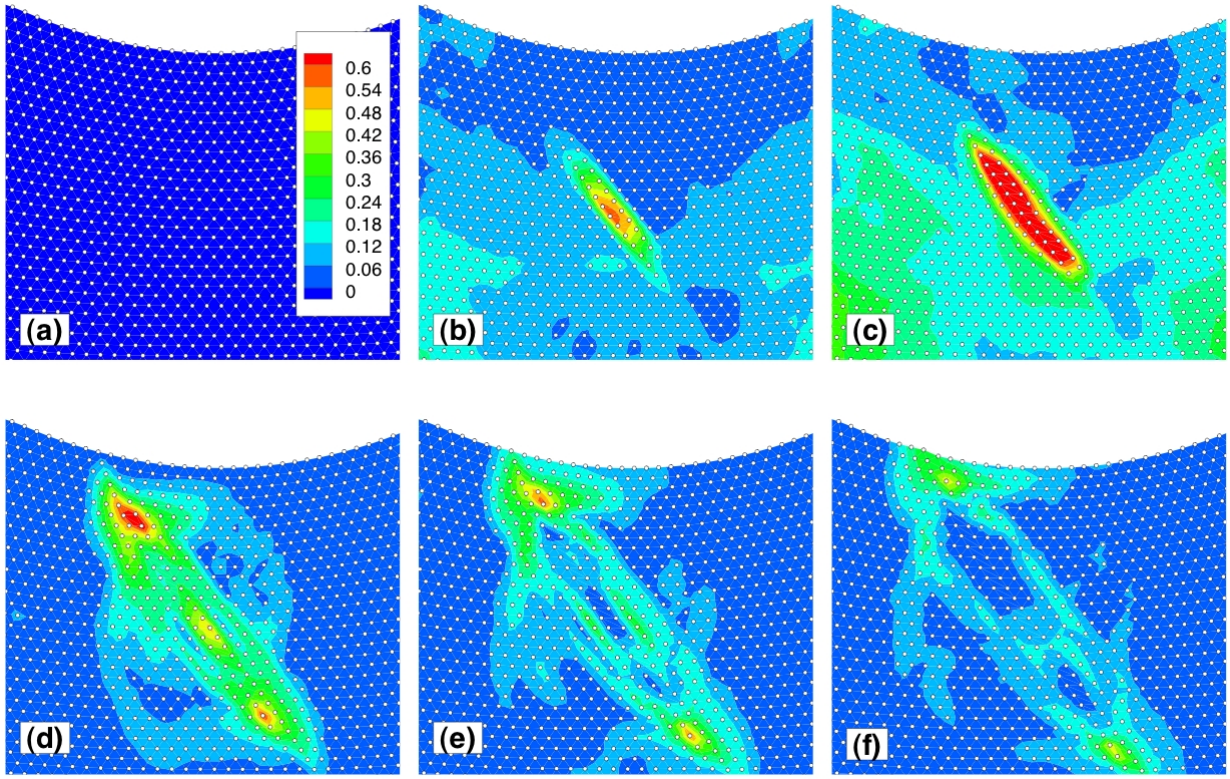

Figure 6: Nucleation and motion of a dislocation dipole during nano-indentation, with contours showing relative magnitudes of atomic motion (**Å)**. (a) the undefected cystal. (b) nucleation (c) growth to a full Burgers vector and (d)-(f) motion.

Figures 5 and 6 illustrate the differences between nucleation and motion by showing selected snapshots of the atomistic configurations as the dislocation dipole nucleates and moves. In Fig. 5, we show the atoms and a mesh between them. The crystal in figure 5(a) is defect free, and the nucleation step is shown in (b). From (b) to (c) the dislocation dipole develops a full Burgers vector, but the two dislocations do not move substantially. Finally, frames (d)-(f) show the dipole growing as the two dislocation break free of each other and move apart. Arrows in each frame show the approximate width of the dipole.

Figure 6 shows the same atomic configurations as in figure 5, but superimposed on contours of the magnitude of relative atomic motion between subsequent images. For example, contours in frame (b) show the change in atomic positions during the motion from configuration (a) to (b). It is clear that the nucleation and growth phase (frames (b) and (c)) involve the collective sliding of atoms over two planes, as described previously in the discussion of nucleation. By contrast, the dislocation motion shown in frames (d) through (f) is accomplished by localized rearrangements within the dislocation cores, thus the relatively small regions of red contours at either end of the dipole.

3. FDM and MFDM

The presence of dislocations and applied loads induce stresses in a body. The nucleation and motion of dislocations induce permanent deformation in the body. The evolution of the defect

distribution and the stress field are intimately coupled, each affecting the other. The primary goal of the theory of Field Dislocation Mechanics (FDM, Acharya, 2001, 2003, 2004) is to achieve a mathematical description of this process. Its equations may be written in the form

$$\begin{aligned} &curl\,\boldsymbol{\chi} = \boldsymbol{\alpha} \\ &div\,\boldsymbol{\chi} = \boldsymbol{0} \\ &div\big(grad\,\dot{\boldsymbol{z}}\big) = div\big(\boldsymbol{\alpha}\times\boldsymbol{V} + \boldsymbol{\Omega}\big) \\ &div\Big[\boldsymbol{C} : \big\{grad\,(\boldsymbol{u}-\boldsymbol{z}) + \boldsymbol{\chi}\big\}\Big] + \boldsymbol{b} = \boldsymbol{0} \\ &\dot{\boldsymbol{\alpha}} = -curl\,(\boldsymbol{\alpha}\times\boldsymbol{V}) + \boldsymbol{s}. \end{aligned} \tag{1}$$

Here, $\boldsymbol{\chi}$ is the incompatible part of the elastic distortion tensor $\boldsymbol{U}^e$, $\boldsymbol{u}$ is the total displacement field, $\boldsymbol{u}-\boldsymbol{z}$ is a vector field whose gradient is the compatible part of the elastic distortion tensor, $\boldsymbol{C}$ is the fourth-order, possibly anisotropic, tensor of linear elastic moduli, $\boldsymbol{b}$ is the body force per unit volume field, $\boldsymbol{\alpha}$ is the dislocation density tensor, $\boldsymbol{V}$ is the dislocation velocity vector, $\boldsymbol{s}$ is a dislocation nucleation rate tensor (not related to dislocation line length increase from *existing* dislocations), and $\boldsymbol{\Omega}$ a rate of slipping tensor representing the slip associated with dislocation nucleation. On the other hand, $\boldsymbol{\alpha}\times\boldsymbol{V}$ represents the slip rate associated with the motion of existing dislocations. The argument of the div operator in $(1)_4$ is the stress tensor, and the functions $\boldsymbol{V}$, $\boldsymbol{s}$, $\boldsymbol{\Omega}$ are constitutively specified.

These equations admit well-defined initial and boundary conditions that have been worked out (Acharya 2003, Acharya and Roy, 2006). In particular, $(1)_{1,2,3}$ are solved with the essential conditions

$$\begin{aligned} &\boldsymbol{\chi}\boldsymbol{n} = \boldsymbol{0} \ \text{ on } \ \partial B \\ &\boldsymbol{z} \text{ arbitrarily fixed at one point of the body} \end{aligned} \tag{2}$$

(only $grad\,\boldsymbol{z}$ is of physical importance) and $(1)_3$ implies the natural condition at the boundary given by

$$\big(grad\,\dot{\boldsymbol{z}} - \boldsymbol{\alpha}\times\boldsymbol{V} - \boldsymbol{\Omega}\big)\boldsymbol{n} = \boldsymbol{0} \ \text{ on } \ \partial B. \tag{3}$$

Here, $\boldsymbol{n}$ refers to the outward normal field on the boundary of the body. In this model of dislocation mechanics, the total displacement does not represent the actual physical motion of atoms involving topological changes but only a consistent shape change and hence is not required to be discontinuous. However, the stress produced by these topological changes in the lattice is adequately reflected in the theory through the utilization of incompatible elastic/plastic distortions. Indeed, the compatible part (i.e. a part that can be represented as a gradient of a vector field) of the plastic distortion is given by $grad\,\boldsymbol{z}$ and the total displacement gradient is simply the sum of the compatible parts of the elastic and plastic distortions:

$$grad\,\boldsymbol{u} = \big(\boldsymbol{U}^e - \boldsymbol{\chi}\big) + grad\,\boldsymbol{z}\,. \tag{4}$$

To derive the structure of an averaged theory (Mesoscopic Field Dislocation Mechanics, MFDM) corresponding to (1), we adapt a commonly used averaging procedure utilized in the study of multiphase flows (e.g. Babic, 1997) for our purposes. For a microscopic field f given as a function of space and time, we define the mesoscopic space-time averaged field $\overline{f}$ as follows:

$$\bar{f}(\boldsymbol{x},t) := \frac{1}{\int_{I(t)}\int_{\Omega(\boldsymbol{x})} w\left(\boldsymbol{x}-\boldsymbol{x}',t-t'\right)\, d\boldsymbol{x}'dt'} \int_{\Im}\int_{B} w\left(\boldsymbol{x}-\boldsymbol{x}',t-t'\right) f\left(x',t'\right) d\boldsymbol{x}'dt', \tag{5}$$

where B is the body and $\Im$ a sufficiently large interval of time. In the above, $\Omega(\boldsymbol{x})$ is a bounded region within the body around the point $\boldsymbol{x}$ with linear dimension of the order of the spatial resolution of the macroscopic model we seek, and $I(t)$ is a bounded interval in $\Im$ containing t. The averaged field $\bar{f}$ is simply a weighted, space-time, running average of the microscopic field f. The weighting function w is non-dimensional, assumed to be smooth in the variables $\boldsymbol{x},\boldsymbol{x}',t,t'$ and, for fixed $\boldsymbol{x}$ and t, have support (i.e. to be non-zero) only in $\Omega(\boldsymbol{x})\times I(t)$ when viewed as a function of $(\boldsymbol{x}',t')$. Applying this operator to the equations in (1), we obtain [9] an *exact* set of equations for the averages given as

$$\begin{aligned}
&curl\,\bar{\boldsymbol{\chi}} = \bar{\boldsymbol{\alpha}}\\
&div\,\bar{\boldsymbol{\chi}} = \boldsymbol{0}\\
&div\left(grad\,\dot{\bar{\boldsymbol{z}}}\right) = div\left(\bar{\boldsymbol{\alpha}}\times\bar{\boldsymbol{V}} + \boldsymbol{L}^p\right)\\
&\bar{\boldsymbol{U}}^e = grad\left(\bar{\boldsymbol{u}}-\bar{\boldsymbol{z}}\right)+\bar{\boldsymbol{\chi}}\\
&div\,\bar{\boldsymbol{T}} = \boldsymbol{0}\\
&\dot{\bar{\boldsymbol{\alpha}}} = -curl\left(\bar{\boldsymbol{\alpha}}\times\bar{\boldsymbol{V}} + \boldsymbol{L}^p\right)
\end{aligned} \tag{6}$$

where $\boldsymbol{L}^p$, defined as

$$\boldsymbol{L}^p(\boldsymbol{x},t) := \overline{(\boldsymbol{\alpha}-\bar{\boldsymbol{\alpha}})\times\boldsymbol{V}}(\boldsymbol{x},t) = \overline{\boldsymbol{\alpha}\times\boldsymbol{V}}(\boldsymbol{x},t) - \bar{\boldsymbol{\alpha}}(\boldsymbol{x},t)\times\bar{\boldsymbol{V}}(\boldsymbol{x},t), \tag{7}$$

and $\bar{\boldsymbol{V}}$ are the terms that require closure (and we have ignored the terms $\bar{\boldsymbol{s}}$ and $\bar{\boldsymbol{\Omega}}$ for simplicity). Physically, $\boldsymbol{L}^p$ is representative of a portion of the average slip strain rate produced by the 'microscopic' dislocation density; in particular, it can be non-vanishing even when $\bar{\boldsymbol{\alpha}} = \boldsymbol{0}$ and, as such, it is to be physically interpreted as the strain-rate produced by so-called 'statisticaldislocations' (SD), as is also indicated by the extreme right-hand side of (7). The variable $\bar{\boldsymbol{V}}$ has the obvious physical meaning of being a space-time average of the pointwise, microscopic dislocation velocity. Initial and boundary conditions for (6) are important from the physical modeling point of view, particularly in the context of triggering inhomogeneity under boundary conditions corresponding to homogeneous deformation in conventional plasticity theory. These have also been worked out (Acharya and Roy, 2006).

4. Physical interpretation of driving force for dislocation nucleation

In this section we derive the driving forces for dislocation nucleation and motion implied by FDM along with a global, mechanical version of the Second Law of thermodynamics. We then physically interpret the driving force for nucleation. The physical interpretation of the driving force for motion was provided in Acharya (2003) establishing it as an analog, in the field setting, of the Peach-Koehler force of classical dislocation theory. Due to the nonlocal nature of the theory, the derivation requires a mathematical device for decomposing the stress field into compatible and incompatible parts. In Acharya (2001, 2003, 2004), orthogonal decompositions for merely square-integrable $\left(L^2(B)\right)$ fields are used. At the cost of using less smooth functions

but to make the analogy with classical Stokes-Helmholtz decompositions of $H^1(B)$ tensor fields on bounded domains, we utilize the following theorem due to Friedrichs (cf. Jiang, 1998, Thm 5.8, 5.2): Given a sufficiently smooth $\left(H^1(B)\right)$ stress field $\boldsymbol{T}$, there exists a unique tensor field $\boldsymbol{W}$ satisfying

$$\begin{aligned} &div\,\boldsymbol{W} = \boldsymbol{0} \text{ on } B \\ &\boldsymbol{W}\times\boldsymbol{n} = \boldsymbol{0} \text{ on } \partial B \end{aligned} \tag{8}$$

and a unique vector field $\boldsymbol{g}$ satisfying

$$(grad\,\boldsymbol{g} - \boldsymbol{T})\boldsymbol{n} = \boldsymbol{0} \text{ on } \partial B, \tag{9}$$

such that

$$\boldsymbol{T} = curl\,\boldsymbol{W} + grad\,\boldsymbol{g} \tag{10}$$

and the orthogonality condition

$$\int_B grad\,\boldsymbol{g} : curl\,\boldsymbol{W}\, dv = 0 \tag{11}$$

holds. In passing, we note that the boundary condition $(8)_2$ implies $(curl\,\boldsymbol{W})\boldsymbol{n} = \boldsymbol{0}$ on ∂B, a condition that is useful in proving the decomposition (10).

The use of this Stokes-Helmholtz decomposition of the stress field in the derivation that follows immediately is an effort to state precisely the following observation: defining

$$\boldsymbol{U}^p := grad\,\boldsymbol{u} - \boldsymbol{U}^e = grad\,\boldsymbol{z} - \boldsymbol{\chi} \text{ and } \boldsymbol{s} = -curl\,\boldsymbol{\Omega}$$

so that

$$curl\,\dot{\boldsymbol{U}}^p = -\dot{\boldsymbol{\alpha}} = curl\,(\boldsymbol{\alpha}\times\boldsymbol{V} + \boldsymbol{\Omega})$$

it seems reasonable to want to conclude that the rate of plastic working in the body

$$\int_B \boldsymbol{T} : \dot{\boldsymbol{U}}^p dv \cong \int_B \boldsymbol{T} : (\boldsymbol{\alpha}\times\boldsymbol{V} + \boldsymbol{\Omega})\, dv\,.$$

The rate of working of the external loads less the rate of change of free energy of the body yields the rate at which mechanical energy is dissipated:

$$D = \int_{\partial B} (\boldsymbol{T}\boldsymbol{n})\cdot\dot{\boldsymbol{u}}\, da + \int_B \boldsymbol{b}\cdot\dot{\boldsymbol{u}}\, dv - \frac{d}{dt}\int_B \psi\, dv. \tag{12}$$

We assume that the specific free energy depends only on the symmetric part of the elastic distortion and the stress is given by the derivative of the free energy with respect to its argument, i.e.

$$\psi = \psi\left(\boldsymbol{U}^e_{sym}\right) \quad ; \quad \boldsymbol{T} = \frac{\partial\psi}{\partial\boldsymbol{U}^e_{sym}}. \tag{13}$$

Equations (12), (13), (4), and (10) now imply

$$D = \int_B \boldsymbol{T} : (grad\,\dot{\boldsymbol{z}} - \dot{\boldsymbol{\chi}})\, dv = \int_B (curl\,\boldsymbol{W} + grad\,\boldsymbol{g}) : (grad\,\dot{\boldsymbol{z}} - \dot{\boldsymbol{\chi}})\, dv\,. \tag{14}$$

Utilizing the conditions $(8)_2$, $(2)_1$, $(1)_2$, the dissipation simplifies to

$$D = \int_B grad\,\boldsymbol{g} : grad\,\dot{\boldsymbol{z}}\, dv - \int_B curl\,\boldsymbol{W} : \dot{\boldsymbol{\chi}}\, dv\,. \tag{15}$$

Furthermore, (3) and $(1)_3$ imply

$$\int_B grad\,\boldsymbol{g} : grad\,\dot{\boldsymbol{z}}\, dv = \int_B grad\,\boldsymbol{g} : (\boldsymbol{\alpha}\times\boldsymbol{V} + \boldsymbol{\Omega})\, dv\,, \tag{16}$$

and $(8)_2$, and $(1)_{1,5}$ imply

$$\int_B curl\,\boldsymbol{W} : \dot{\boldsymbol{\chi}}\, dv = \int_B \boldsymbol{W} : \boldsymbol{s}\, dv - \int_B curl\,\boldsymbol{W} : (\boldsymbol{\alpha}\times\boldsymbol{V})\, dv, \tag{17}$$

so that the dissipation in the model may be expressed as

$$D = \int_B \boldsymbol{T} : \boldsymbol{\alpha}\times\boldsymbol{V}\, dv + \int_B -\boldsymbol{W} : \boldsymbol{s}\, dv + \int_B grad\,\boldsymbol{g} : \boldsymbol{\Omega}\, dv. \tag{18}$$

Based on the physical meaning of a dislocation being the boundary between slipped regions of differing magnitude, it seems natural to associate the dislocation nucleation rate $\boldsymbol{s}$ with an appropriate, incompatible measure of the spatial variation of the nucleation slipping rate $\boldsymbol{\Omega}$, i.e.

$$\boldsymbol{s} = -curl\,\boldsymbol{\Omega}, \tag{19}$$

which also satisfies the requirement that the dislocation density field $\boldsymbol{\alpha}$ be divergence-free. Then,

$$D = \int_B \left(\boldsymbol{X}(\boldsymbol{T}\boldsymbol{\alpha})\cdot\boldsymbol{V} + \boldsymbol{T} : \boldsymbol{\Omega}\right) dv, \tag{20}$$

where $\left\{\boldsymbol{X}(\boldsymbol{T}\boldsymbol{\alpha})\right\}_i = \varepsilon_{ijk} T_{jr} \alpha_{rk}$ and ε_{ijk}, for specific values of the indices, is a Cartesian component of the third-order alternating tensor. The form of (20) suggests the driving forces for the dissipative mechanisms of dislocation motion characterized by the dislocation velocity $\boldsymbol{V}$ and nucleation slip characterized by $\boldsymbol{\Omega}$ as $\boldsymbol{X}(\boldsymbol{T}\boldsymbol{\alpha})$ and $\boldsymbol{T}$, respectively.

The physical content of the driving force for dislocation motion has been dealt with in detail in Acharya (2003). In order to gain physical insight into possible constitutive equations for nucleation suggested by the theory, let the strain rate associated with the nucleation event be written as

$$\boldsymbol{\Omega} = \varsigma\, \boldsymbol{m} \otimes \boldsymbol{n}$$

where $\boldsymbol{m}$ is slip (burgers) vector direction, $\boldsymbol{n}$ is the slip plane normal and ς is a scalar rate of slipping. Substituting in (20), the driving force for nucleation on a slip plane is given by

$$\boldsymbol{m}\cdot\boldsymbol{T}\boldsymbol{n} =: \tau,$$

the traction on the slip plane resolved in the direction of the Burgers vector. A simple constitutive assumption for the nucleation slip rate might be

$$\boldsymbol{\Omega} = f(\tau)\boldsymbol{m} \otimes \boldsymbol{n},$$

where f is a non-negative function guaranteeing positive dissipation due to nucleation. Then,

$$\boldsymbol{s} = -\boldsymbol{m} \otimes \left(f'(\tau)\, grad\,\tau \times \boldsymbol{n}\right) \tag{21}$$

by definition, and thus the theory suggest that a dislocation line appears where there is a sizeable gradient of the resolved traction, but only in directions *along* the slip plane. Gradients in the out-of-plane directions are immaterial for the purposes of nucleation. Given the definition of a dislocation line as a boundary between unequally slipped regions on a slip plane, this makes physical sense if we relate magnitude of slipping at a point to be in proportion to the resolved traction at that point.

The use of (21) in a nanoscale continuum theory would require a physically accurate definition and constitutive representation of the stress tensor at the nanoscale. In particular, the stress field resulting from such a description would have to be able to represent spatial heterogeneity at the scale of a lattice spacing. These are delicate issues as reflected in the considerations of Machova (2001), Nielsen and Martin (1985), Cormier et al. (2001), Lutsko (1988), Hardy (1982), Irving and Kirkwood (1950), Tsai (1979) and Maranganti et al. (2007).

5. Plastic front propagation in PMFDM

In this section we demonstrate the capability of the phenomenological MFDM (PMFDM) framework in representing the phenomena of propagating fronts of plastic deformation. Experimental studies on a number of metals suggest that "self excited waves" may be ubiquitous in plastic flow (Zuev, 2006). Kocks (1981) pointed out that the spreading of a Lüder's front is actually a delocalization following an initial instability. While the prediction of the propagation of plastic fronts has been a long-time goal of 3-d plasticity theory, the realization of such a goal is hampered by the mathematical structure forwarded in the traditional approach to analysis. Within the conventional theory, propagating fronts of plastic deformation can be obtained in the presence of spatial variations in material properties (e.g. polycrystals, spatial variations in strength etc.); however, such fronts are also observed in single crystals with spatially homogeneous hardening characteristics (Zeigenbein et al., 1995). Generally speaking, the progression of waves is properly identified with the phenomenon of transport and concomitant description through partial differential equations. In what follows, we present the qualitative prediction of a plastic wave following from transport of excess dislocation density.

We note that for a model at the mesoscale it is physically essential to introduce realistic constitutive assumptions for the plastic strain rate produced by the unresolved statistical density and the average velocity of the excess density; below, we outline one such model. However, we emphasize that the qualitative prediction of the moving plastic front is insensitive to the choice of any such model (as long as it incorporates a mechanism for initial softening, here through rapid evolution of the statistical mobile density), and is a direct result of the transport in excess dislocation density implied by the field equation $(6)_6$.

The propagation of a Lüder's band in solid solution alloys is typically associated the microscale mechanism of mobile dislocation breakaway from solute atoms. The macroscale response is reflected in the development of a yield point and the propagation of a plastic front. Lüder's band propagation has also been noted in whisker crystals of pure fcc metals (Brenner 1957; Nittono 1971). The tensile stress-strain curve of copper whiskers includes a sharp yield point followed by a region of easy glide, leading finally to a work hardening response. The propagation of slip ahead of the Lüder's band is generally associated with the mechanism of cross-slip (Brenner 1957; Nittono 1971). The kinetics of deformation in copper whiskers was investigated by Saimoto (1960) through incremental loading applied at different test temperatures. Gotoh (1974) observed that the yield point drop occurred at the point in which an initial slip line is crossed by another and noted double cross-slip as a mechanism of band propagation in [110] single crystals.

In the following, we outline a PMFDM model for the tensile deformation of a flat whisker. The averaged slip strain rate $\boldsymbol{L}^p$ follows from the activity of statistical mobile dislocations on the 12 fcc slip systems as

$$\boldsymbol{L}^p = \sum_s \rho_m b v_s \boldsymbol{b}_s \otimes \boldsymbol{m}_s \tag{22}$$

where ρ_m is the statistical mobile density, $\boldsymbol{b}_s$ and $\boldsymbol{n}_s$ are the Burgers vector and normal of slip system s, b is the magnitude of the Burgers vector and v_s is an averaged velocity (to be detailed below). We adopt evolution relations as outlined in Varadhan *et al.* (2005), with simplifications deemed appropriate for the relatively limited range of straining considered in the present simulations. For the statistical mobile density there is generation and loss according to

$$\dot{\rho}_m = \left(\frac{C_1}{C_2} - C_2 \rho_m \right) \dot{\Gamma} , \tag{23}$$

where $\dot{\Gamma}$ is the rate of straining due to the combined action of statistical and excess mobile dislocation densities given by

$$\dot{\Gamma} = \left| \bar{\boldsymbol{\alpha}} \times \bar{\boldsymbol{V}} \right| + \sum_s \rho_m b \left| v_s \right| . \tag{24}$$

The creation of forest (sessile) dislocation density, ρ_f, follows from interaction with excess dislocations (Acharya and Beaudoin, 2000) and loss of mobile density

$$\dot{\rho}_f = \frac{C_0}{b} \sum_s \left| \bar{\boldsymbol{\alpha}} \cdot \boldsymbol{n}_s \right| \left(\rho_m b \left| v_s \right| + \left| \bar{\boldsymbol{\alpha}} \times \bar{\boldsymbol{V}} \right| \right) + C_2 \rho_m \dot{\Gamma} . \tag{25}$$

In the above C_0, C_1 and C_2 are material constants.

The ensemble velocity for statistical densities follows the power law relation

$$v_s = v_0 \left(\frac{\left| \tau_s \right|}{\tau_a + \tau_h} \right)^m \operatorname{sgn}\left(\tau_s \right) \quad ; \quad \tau_s = \left(\boldsymbol{b}_s \otimes \boldsymbol{n}_s \right) : \boldsymbol{T} \tag{26}$$

with reference velocity v_0, athermal strength τ_a and stress exponent m as material parameters and the hardness τ_h related to the forest density in the usual way as

$$\tau_h = aGb\sqrt{\rho_f} , \tag{27}$$

where a is a non-dimensional material parameter and G is the shear modulus.

The excess density is transported with the velocity

$$\bar{\boldsymbol{V}} = v \boldsymbol{d} / \left| \boldsymbol{d} \right| \tag{28}$$

whose magnitude is assumed to be an average of the statistical slip velocities over the $n = 12$ slip systems

$$v = \frac{1}{n} \sum_s \left| v_s \right| , \tag{29}$$

and the direction is prescribed as (Acharya and Roy, 2006)

$$\begin{aligned} &\boldsymbol{d} := \boldsymbol{b} - \left(\boldsymbol{b} \cdot \frac{\boldsymbol{a}}{|\boldsymbol{a}|} \right) \frac{\boldsymbol{a}}{|\boldsymbol{a}|} , \\ &\boldsymbol{b} := \boldsymbol{X}\left(\bar{\boldsymbol{T}}' \bar{\boldsymbol{\alpha}} \right) \ ; \ b_i = e_{ijk} \bar{T}'_{jr} \bar{\alpha}_{rk} \quad ; \quad \boldsymbol{a} := \boldsymbol{X}\left(tr\left(\bar{\boldsymbol{T}} \right) \bar{\boldsymbol{\alpha}} \right) \ ; \ a_i = \left(\frac{1}{3} \bar{T}_{mm} \right) e_{ijk} \bar{\alpha}_{jk} . \end{aligned} \tag{30}$$

Note that while $\bar{\boldsymbol{V}}$ is not constrained to a slip plane, however, the character of excess density dislocation following from the contribution $-curl\, \boldsymbol{L}^p$ in $(6)_6$ follows from slip geometry. This leads to "generation" of Burgers vector and line direction in $\bar{\boldsymbol{\alpha}}$ with crystallographic sense. In turn, the relation (30) leads to transport of the excess density in roughly the sense that one would expect from the Peach-Koehler relation (Acharya, 2003). This was demonstrated in modeling of the torsion of ice single crystals (Taupin *et al*., 2007), where the predominant movement of screw dislocations developed in torsion was on basal planes. The interplay of internal stresses associated with $\bar{\boldsymbol{\chi}}$ and the applied stress may indeed provide a driving force with (30) allowing for transport out of the slip plane. Such role is critical in the present work to representing a mechanism of transport of excess dislocation density along the specimen axis.

The sample geometry and orientation studied by Nittono (1971) serve as a basis for the present

Table 1 – Material parameters used in the whisker simulation

b	0.26 [nm]	v_0	$3.5 \cdot 10^{-8}$ [m/s]
C_0	25.0	α	0.35
C_1	2.43E-05	ν	0.42
C_2	3.03	$\rho_f(0)$	10^{10} [m^{-2}]
E	66.6 [GPa]	$\rho_m(0)$	10^{8} [m^{-2}]
G	75.2 [GPa]	τ_a	3.7 [MPa]
m	20		

study. The whisker cross-section was taken as 200 μm in width by 30 μm in thickness. Total length was 2400 μm with degrees of freedom fully constrained on one end and velocity in the

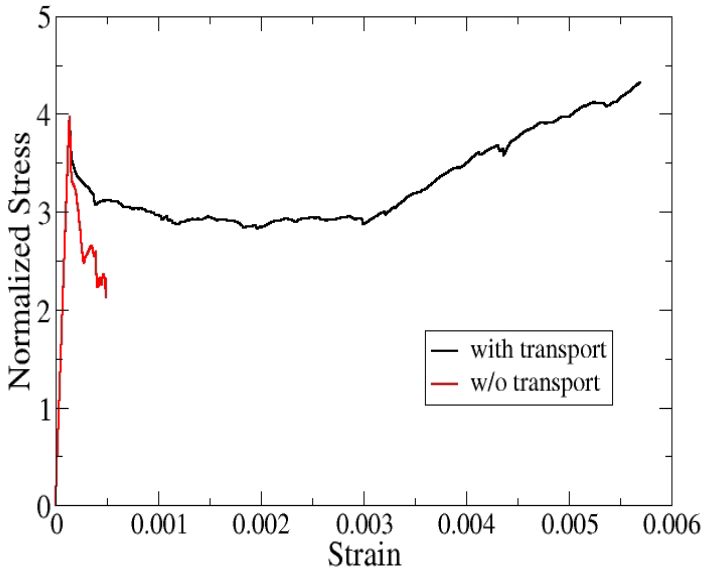

Figure 7: Stress-strain response, with flow stress normalized by the initial slip system strength.

direction of elongation only applied at the other. The applied strain rate is 10^{-3} sec^{-1}. The mesh

contained 24, 6 and 192 elements in the width, thickness and length directions, respectively. The finite element formulation outlined in references (Roy and Acharya, 2006; Varadhan *et al.* 2005) was adopted with linear interpolation used for the $\bar{\chi}$ field and quadratic interpolation used for

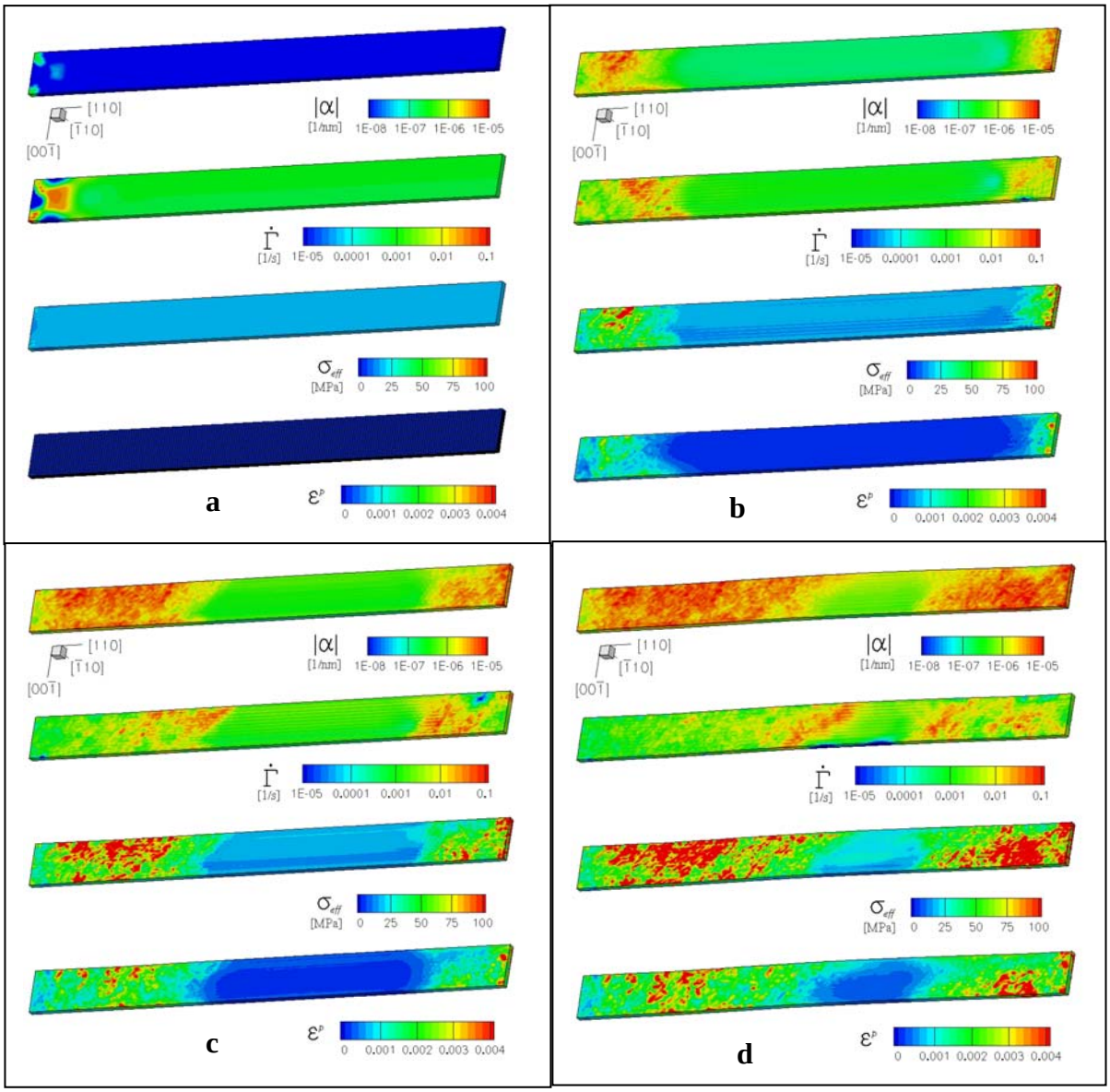

Figure 8 – Magnitude of the excess density, rate of plastic strains, effective stress and effective plastic strain at nominal strains of a) $\varepsilon = 0.00016$, b) $\varepsilon = 0.0007$, c) $\varepsilon = 0.0016$ and d) $\varepsilon = 0.0026$.

the $\bar{\boldsymbol{z}}$ and $\bar{\boldsymbol{u}}$ fields. This choice of interpolation provides for a piecewise linear continuity in evaluation of the elastic distortion $\bar{\boldsymbol{U}}^{\boldsymbol{e}}$ and allied stresses. Anisotropic elastic response is described through Young's modulus, *E*, Poisson's ratio, ν, and shear modulus, G. The transport problem, $(6)_6$, is addressed using the Galerkin-Least Squares treatment given by Varadhan *et al.* (2006), with added diffusion that is consistent from the numerical perspective. Parameters used

in the simulation are listed in Table 1. The stress strain response is shown in Fig. 7 for simulations with transport of the excess density $\bar{\boldsymbol{\alpha}}$, as outlined above, and without transport of the excess density, by setting $\bar{\boldsymbol{V}} = \boldsymbol{0}$. In both cases, there is elastic loading followed by a stress drop, associated with the evolution of statistical mobile density. With transport, this stress drop is followed by plateau, then a transition to a work hardening response. Without transport, the initial development of plastic strain rate, associated with the stress drop, is similar to that shown in Figure 8a. However, subsequent plastic activity does not spread throughout the specimen, localization follows, and the calculation can only be continued up to an applied strain of $\sim 5\times10^{-4}$ before the time-steps become prohibitively small.

The progression of deformation with transport is shown in Fig. 8. Initial plastic activity, indicated by the strain rate measure $\dot{\Gamma}$, develops in a relatively symmetric fashion at the left end of the specimen (Fig. 8a). Slip then progresses from left to right, with a relatively diffuse region of slip activity. A second plastic front develops at the right end of the specimen, moving from right to left. The magnitude of the plastic strain is taken as $\varepsilon^p = \sqrt{2/3\left(\bar{\boldsymbol{U}}^p : \bar{\boldsymbol{U}}^p\right)}$, where $\bar{\boldsymbol{U}}^p = -\bar{\boldsymbol{\chi}} + \mathit{grad}\,\bar{\boldsymbol{z}}$. Slip progresses through the specimen volume by the motion of these plastic fronts. The history of non-uniform plastic activity is indicated by the magnitude of the excess density, $|\bar{\boldsymbol{\alpha}}|$, progressing with a relatively sharp front. Plastic activity exists ahead of the excess density front over a distance on the order of hundreds of μm.

In this small displacement gradient formulation, stress concentrations arising from geometric defects such as slip steps are not represented. However, localized internal stress arising from slip incompatibilities are captured through $(6)_1$ and the subsequent stress calculation. One can see that the stress at the head of the front is elevated with respect to the nominal stress in the (relatively) undeformed cross-section (Fig. 8a-8d). This higher stress at the head of the plastic front is more representative of the upper yield stress developed after initial elastic loading and not the lower yield stress associated with the plateau. This notion was set forth by Ziegenbein *et al*. (1995) in a study of solution-strengthened Cu single crystals. The present result suggests that stress concentrations associated with incompatibilities play a role in setting stress at the head of a propagating band.

With the mesoscale averaged response implied in the present simulations, one cannot draw association of observations made in the simulation with specific microstructural mechanism. Specifically, associating the symmetric pattern of plastic activity in Fig. 8a with initiation of a plastic front following from slip on two planes (and thereby rendering double cross-slip) (Gotoh 1974) or deeming the diffuse region of strain rate to be due to preceding dislocations (Nittono 1971) is to overstate the detail represented in the simulation. On the other hand, the PMFDM setting allows one to adopt established models of crystal plasticity and work hardening and cast such within an overarching framework that allows for the transport of dislocation content from one point in the specimen to another. The resulting partial differential equations provide for development of a propagating plastic front, without resort to *ad hoc* extensions of the local models to provide for spatial coupling.

6. Implication of macroscopic plasticity as a limit of MFDM: a new continuity condition

MFDM is a model of plasticity that forges a precise link between the classical theories of *elasto-plasticity* and *continuously distributed dislocations***,** based on averaging the latter to obtain an

augmentation of the former. The two classical approaches have been pursued (historically) by separate groups of researchers with different research objectives; more importantly, while there has been strong appreciation amongst researchers of the fact that the two classical theories must somehow be related, a sound mathematical model with physically rigorous underpinnings has eluded the community for forty-odd years.

To see the link that MFDM introduces, we consider the usual equations for equilibrium and linear elasticity,

$$div\,\boldsymbol{T} = \boldsymbol{0} \tag{31}$$

and

$$\boldsymbol{T} = \boldsymbol{C} : \boldsymbol{U}^e \tag{32}$$

where $\boldsymbol{T}, \boldsymbol{C}, \boldsymbol{U}^e$ are the Cauchy stress, fourth-order tensor of linear elastic moduli and elastic distortion. For simplicity, here we restrict attention to the small-deformation case.

In classical elastoplasticity theory the elastic distortion is assumed to arise as the difference of the total displacement gradient and the plastic distortion given by

$$\boldsymbol{U}^e = grad\,\boldsymbol{u} - \boldsymbol{U}^p, \tag{33}$$

and the rate of plastic distortion is prescribed by a constitutive model:

$$\dot{\boldsymbol{U}}^p = \boldsymbol{L}^p. \tag{34}$$

For example, in von-Mises J_2 plasticity the plastic strain rate is specified as

$$\boldsymbol{L}^p = \dot{\gamma}\,\boldsymbol{T}'$$

where $\dot{\gamma}$ is an appropriately defined scalar measure of plastic strain rate and $\boldsymbol{T}'$ is the stress deviator; in crystal plasticity it is a description of slipping on predefined slip systems as

$$\dot{\boldsymbol{U}}^p = \boldsymbol{L}^p = \sum_{\kappa} \dot{\gamma}^{\kappa} \boldsymbol{b}^{\kappa} \otimes \boldsymbol{n}^{\kappa}. \tag{35}$$

where $\dot{\gamma}^{\kappa}$ is the slip system shearing rate on the system κ dependent upon stress and strength, and $\boldsymbol{b}^{\kappa}$ and $\boldsymbol{n}^{\kappa}$ are the individual slip system directions and normals, respectively. In these classical theories, the slipping rate is a local function of stress, strength (and strain rate, in the rate-independent case).

These classical models have been shown to be versatile in the prediction of overall shape changes due to permanent deformation. However, they cannot deal with the question of predicting the internal stress field of dislocation distributions in the material.

On the other hand, in the classical theory of continuously distributed dislocations (Kröner, 1981; Mura, 1963) the equations (31)-(32) are solved along with the equation

$$curl\,\boldsymbol{U}^e = \boldsymbol{\alpha} \tag{36}$$

where $\boldsymbol{\alpha}$ is assumed to be a pre-assigned field of dislocation density (Nye's dislocation density tensor, Nye, 1953). Thus, this theory predicts the internal stress of the dislocation density distribution but is silent on the matter of predicting permanent deformation. Mura (1963), following Kröner, also suggested the following equation of evolution for the dislocation density,

$$\dot{\boldsymbol{\alpha}} = -curl\left(\boldsymbol{\alpha} \times \boldsymbol{V}\right), \tag{37}$$

where $\boldsymbol{V}$ is the microscopic dislocation velocity, but realized that this equation could not be the correct one at averaged scales. In the context of this discussion, it is important to realize that the classical theory of elastoplasticity implies the following equation for the evolution of dislocation density

$$\dot{\boldsymbol{\alpha}} = -curl\left(\boldsymbol{L}^p\right) \tag{38}$$

MFDM averages the microscopic equation (37) of evolution of dislocation density to show that, to first order, the natural equation for evolution of dislocation density at mesoscopic and higher scales should be (*ignoring the overhead bars for convenience in this section*)

$$\dot{\boldsymbol{\alpha}} = -curl\left(\boldsymbol{\alpha}\times\boldsymbol{V} + \boldsymbol{L}^p\right). \tag{39}$$

where $\boldsymbol{\alpha}\times\boldsymbol{V}$ is the *microplastic strain rate* associated with the motion of signed, *excess dislocation density* and $\boldsymbol{L}^p$ is the strain rate associated with statistical density of no net sign. Due to the fact that (39) is a conservation law for essentially a density of lines, an observation that makes sense due to the definition (36) of $\boldsymbol{\alpha}$ as a curl of a tensor field even without an association with crystal dislocations, it implies jump conditions on surfaces of discontinuity (Acharya 2007). In particular, in the simple case of a material surface of discontinuity not moving with respect to the material (39) implies

$$\left[\!\left[\boldsymbol{\alpha}\times\boldsymbol{V} + \boldsymbol{L}^p\right]\!\right]\times\boldsymbol{N} = \boldsymbol{0}, \tag{40}$$

where $[\![\ ]\!]$ represents a jump of its argument at the surface of discontinuity as defined conventionally (Truesdell and Toupin, 1960) and $\boldsymbol{N}$ is the unit normal to the surface, with arbitrarily chosen orientation. The condition implies that the *tangential action of the plastic distortion rate is continuous at a material surface of discontinuity*. Here, given a tensor $\boldsymbol{A}$ and a surface with normal $\boldsymbol{N}$, the tangential action refers to the tensor $\boldsymbol{A} - \boldsymbol{A}\boldsymbol{N}\otimes\boldsymbol{N}$.

In principle, then, the augmentation that MFDM suggests to the classical theory of elastoplasticity [(31)-(34)] is simply the replacement of (34) with

$$\dot{\boldsymbol{U}}^p = \boldsymbol{\alpha}\times\boldsymbol{V} + \boldsymbol{L}^p \tag{41}$$

along with the addition of (39) and (40).

Let us now consider the case where $\boldsymbol{V}\equiv\boldsymbol{0}$ in (41). A complete theory may be stated as

$$\begin{aligned}
&div\,\boldsymbol{T} = \boldsymbol{0}\\
&\boldsymbol{T} = \boldsymbol{C}:\boldsymbol{U}^e\\
&\boldsymbol{U}^e = grad\,\boldsymbol{u} - \boldsymbol{U}^p\\
&\dot{\boldsymbol{U}}^p = \boldsymbol{L}^p\\
&\left[\!\left[\dot{\boldsymbol{U}}^p\right]\!\right]\times\boldsymbol{N} = \left[\!\left[\boldsymbol{L}^p\right]\!\right]\times\boldsymbol{N} = \boldsymbol{0}.
\end{aligned} \tag{42}$$

Apart from $(42)_5$, this is classical plasticity, in particular if the constitutive equation for $\boldsymbol{L}^p$ is local and material length scale independent. *However, appending the jump condition* $(42)_5$ *makes the theory nonlocal as limiting values of fields from two sides of a surface discontinuity are required to have some relationship*. While such a nonlocality does not produce a length-scale effect under self-similar geometric scalings, it does produce a change in the effective plastic strain rate in the theory that is not constitutively specified. For instance, in crystal plasticity theory, active slip system selection at grain boundaries is likely to be affected. In practice, the imposition of $(42)_5$ without a PDE for $\boldsymbol{U}^p$ (or appropriately defined parts of it) is a non-standard matter. Solving equations $(6)_{1-3,5}$ with $\boldsymbol{V}\equiv\boldsymbol{0}$ and their associated jump conditions is one convenient way to ensure that the jump condition $(42)_5$ is imposed. When used in numerical approximation, they also ensure that the spatial heterogeneities in $\boldsymbol{U}^p$ that can produce internal stress are also accounted for in a robust manner.

As an example of the change that this condition implies for predictions of conventional plasticity, we consider the simple case of identifying conditions for deformation localization out of a spatially homogeneous state in small deformation, rate-independent plasticity. The task is to identify the orientation of a surface in a homogeneously deformed, infinite body across which the velocity gradient can experience a jump, with the body continuing to be in static equilibrium. We assume that at all such possible surfaces of discontinuity the material loads plastically on both sides of the discontinuity-surface, i.e., in the parlance of rate-independent plasticity, we consider the linear comparison solid.

Let the constitutive equation for the plastic distortion rate be expressed as

$$\dot{\boldsymbol{U}}^{p} = \left(\boldsymbol{Z} : grad\, \boldsymbol{v}\right)\boldsymbol{Y}\,, \tag{43}$$

where the second-order tensors $\boldsymbol{Z},\boldsymbol{Y}$ are current state dependent and $\boldsymbol{v}$ is the material velocity. The form (43) includes J_2 plasticity and crystal plasticity may be covered with a slight modification. Because of the spatial homogeneity of the current state and the requirement that the velocity be a continuous function, across any possible surface of discontinuity with normal $\boldsymbol{N}$

$$\left[\!\left[\dot{\boldsymbol{U}}^{p}\right]\!\right] = \boldsymbol{Y}\left(\boldsymbol{Z} : \boldsymbol{a}\otimes\boldsymbol{N}\right), \tag{44}$$

where $\boldsymbol{a}$ is an arbitrary vector in the representation $\left[\!\left[grad\, \boldsymbol{v}\right]\!\right] = \boldsymbol{a}\otimes\boldsymbol{N}$. Then,

$$\left[\!\left[\dot{\boldsymbol{U}}^{p}\right]\!\right]\times\boldsymbol{N} = \boldsymbol{0} \Rightarrow \boldsymbol{a}\cdot\boldsymbol{Z}\boldsymbol{N} = 0 \;\text{ or }\; \boldsymbol{Y}\times\boldsymbol{N} = \boldsymbol{0}\,, \tag{45}$$

where $\boldsymbol{N}$ is some direction (to serve as a normal to a candidate plane of discontinuity).

If $\boldsymbol{Y}$ were of the form $\boldsymbol{m}\otimes\boldsymbol{N}$ for some vector $\boldsymbol{m}$, then $\boldsymbol{Y}\times\boldsymbol{N} = \boldsymbol{0}$. For most constitutive equations this requirement would be quite restrictive. For instance, in J_2 plasticity $\boldsymbol{Y}$ is a symmetric deviatoric tensor and this along with the condition $\boldsymbol{Y} = \boldsymbol{m}\otimes\boldsymbol{N}$ implies that $\boldsymbol{m}$ be parallel to $\boldsymbol{N}$, corresponding to the fact that the tensor $\boldsymbol{Y}$ should correspond to a 'uniaxial' state. At any rate, even if the equations of continuing/rate equilibrium lose ellipticity for a $\boldsymbol{Y}$ that is not a rank-one tensor (or, more generally, does not satisfy $\boldsymbol{Y}\times\boldsymbol{N} = \boldsymbol{0}$ for some direction $\boldsymbol{N}$), a bifurcation from a homogeneous state is excluded, assuming strongly-elliptic elasticity. That is, continuing equilibrium requires

$$\left[\!\left[\dot{\boldsymbol{T}}\right]\!\right]\boldsymbol{N} = \boldsymbol{0} \Rightarrow \left(C_{ijkl} - Y_{ij}Z_{kl}\right)N_l N_j\, a_k = 0\,, \tag{46}$$

and even if the set of homogenous linear equations in a_k admit non-trivial solutions in the absence of further constraints, because of the new constraint $(42)_5$ the only admissible solution is $a_k = 0$ in case $\boldsymbol{Y}\times\boldsymbol{N} \neq \boldsymbol{0}$ and the elasticity tensor is strongly elliptic.

Of course, loss of ellipticity implies the loss of strong ellipticity of the equations of equilibrium and under these circumstances unstable behavior in the form of sensitivity to perturbations is to be expected even though non-uniqueness is precluded (for the base state considered). Indeed, it would be interesting to explore to what extent, if at all, the new continuity condition alleviates mesh-sensitivity in computations where the equilibrium equations have lost ellipticity, e.g. softening plasticity. Another curiosity relates to the question of using equation (39) with $\boldsymbol{V} \neq \boldsymbol{0}$ in rate-independent, local, softening plasticity with regard to the alleviation of pathological behavior in computations.

Acknowledgment

AA and AB would like to thank Satya Varadhan for his assistance in carrying out the simulations of Section 5 and review of the manuscript. The financial support of the National Science Foundation through Grant DMI-0423304 is gratefully acknowledged by AA and AB.

References

Acharya, A. 2001. A model of crystal plasticity based on the theory of continuously distributed dislocations, Journal of the Mechanics and Physics of Solids, 49, 761-784.

Acharya, A. 2003. Driving forces and boundary conditions in continuum dislocation mechanics, Proceedings of the Royal Society, A, 459, 1343-1363.

Acharya, A. 2004. Constitutive Analysis of finite deformation field dislocation mechanics, Journal of the Mechanics and Physics of Solids, 52, 301-316.

Acharya, A. 2007. Jump condition for GND evolution as a constraint on slip transmission at grain boundaries, Philosophical Magazine A, 1349-1359.

Acharya, A., Beaudoin, A.J. 2000. Grain-size effect in polycrystals at moderate strains. Journal of the Mechanics and Physics of Solids 48, 2213-2230.

Acharya, A. and Roy, A. 2006 Size effects and idealized dislocation microstructure at small scales: predictions of a phenomenological model of Mesoscopic Field Dislocation Mechanics: Part I, Journal of the Mechanics and Physics of Solids**,** 54, 1687-1710.

Babic, M. 1997. Average balance equations for granular materials. International Journal of Engineering Science, 35, 523-548.

Brenner, S.S., 1957. Plastic deformation of copper and silver whiskers. Journal of Applied Physics 28, 1023-1026.

Dupuy, L., Tadmor, E., Miller, R., Phillips, R., 2005. Finite temperature quasicontinuum: Molecular dynamics without all the atoms. Phys. Rev. Lett. 95, 060202.

Ercolessi, F., Adams, J., 1994. Interatomic potentials from first-principles calculations -- the force-matching method. Europhys. Lett. 26, 583.

Gerberich, W., Tymiak, N., Grunlan, J., Horstemeyer, M., Baskes, M., 2002. Interpretations of indentation size effects. J. Appl. Mech. 69, 433-442.

Gotoh, Y., 1974. Slip patterns of copper whiskers subjected to tensile deformation. Physica Status Solidi (a) 24, 305-313.

Hardy, R. J. 1982. Formulas for determining local properties in molecular-dynamics simulations: shock waves J. Chem. Phys. 76 6228.

Head, A. K., Howison, S. D., Ockendon, J. R., and Tighe, S. P. 1993. An equilibrium theory of dislocation continua. SIAM Review 35, 580-609.

Irving, J. H., Kirkwood J G 1950. The statistical mechanical theory of transport processes: IV. The equations of hydrodynamics J. Chem. Phys. 18 81729

Jiang, B. 1998. The least-squares finite element method. Springer Series in Scientific Computation, Theory and Computation in fluid dynamics and electromagnetics. Springer.

Kelchner, C. L., Plimpton, S., Hamilton, J., 1998. Dislocation nucleation and defect structure during surface indentation. Phys. Rev. B 58(17), 11085-11088.

Knap, J., Ortiz, M., 2001. An analysis of the quasicontinuum method. J. Mech. Phys. Solids. 49, 1899-1923.

Knap, J., Ortiz, M., 2003. Effect of indenter-radius size on Au(001) nanoindentation. Phys. Rev. Lett. 90, 226102.

Kocks U.F., 1981. Kinetics of nonuniform deformation. In: Progress in materials science, Chalmers anniversary volume. Oxford: Pergamon Press; 1981. p. 185.

Kröner, E. 1981. Continuum theory of defects. In *Physics of defects*, ed. R. Balian *et al.*. North Holland Publishing Company, 217-315.

Li, J., Feb 2007. The mechanics and physics of defect nucleation. Mat. Res. Soc. Bulletin 32, 151-159.

Li, J., van Vliet, K., Zhu, T., Yip, S., Suresh, S., 2002. Atomistic mechanisms governing elastic limit and incipient plasticity in crystals. Nature 418, 307-310.
Limkumnerd, S. and Sethna, J. P. 2006a Mesoscale theory of grains and cells: crystal plasticity and coarsening, Phys. Rev. Letters, 96, 095503.
Limkumnerd, S. and Sethna, J. P. 2006b Shocks and slip systems: predictions from a theory of continuum dislocation dynamics. (submitted) available at http://arxiv.org/abs/cond-mat/0610641.
Limkumnerd, S. and Sethna, J. P. 2007 Stress-free states of continuum dislocation fields: Rotations, grain boundaries, and the Nye dislocation density tensor, Phys. Rev. B 75, 224121.
Lutsko J. F. 1988. Stress and elastic constants in anisotropic solids: molecular dynamics techniques J. Appl. Phys. 64 11524.
Machová, A. 2001. Stress calculations on the atomistic level. Modelling Simul. Mater. Sci. Eng. 9, 327-337.
Maranganti, R., Sharma, P. Wheeler, P. 2007. Quantum notions of stress. ASCE Journal of Aerospace Engineering, 22-37.
Miller, R., Acharya, A., 2004. A stress-gradient based criterion for dislocation nucleation in crystals. J. Mech. Phys. Solids 52(7), 1507-1525.
Miller, R.E., Shilkrot, L.E., Curtin, W., 2003. A coupled atomistic and discrete dislocation plasticity simulation of nano-indentation into single crystal thin films. Acta Mat. 52(2), 271-284.
Mura, T. (1970) Individual dislocations and continuum mechanics. In *Inelastic behavior of solids (ed. M. F. Kaninen et al.)*, 211-229. McGraw-Hill.
Nielsen, O. H., Martin, R. M. 1985. Quantum-mechanical theory of stress and force. Phys Rev. B, 32(6), 3780-3791.
Nittono, O., 1971. X-ray topographic studies on the Lüders band propagation and the dislocation motion in copper whisker crystals. Japanese Journal of Applied Physics 10, 188-196.
Nix, W., Gao, H., 1998. Indentation size effects in crystalline materials: a law for strain gradient plasticity. J. Mech. Phys. Solids. 46, 411-425.
Roy, A. and Acharya, A. 2006. Size effects and idealized dislocation microstructure at small scales: predictions of a phenomenological model of Mesoscopic Field Dislocation Mechanics: Part II, Journal of the Mechanics and Physics of Solids**,** 54, 1711-1743.
Roy, A. and Acharya, A. 2005. Finite element approximation of field dislocation mechanics, Journal of the Mechanics and Physics of Solids, 53, 143-170.
Saimoto, S. 1960. Personal communication in reference to "The deformation of copper whiskers," MSc. Thesis, University of British Columbia, Vancouver B.C.
Shenoy, V. B., Miller, R., Tadmor, E., Rodney, D., Phillips, R., Ortiz, M., 1999. An adaptive methodology for atomic scale mechanics: The quasicontinuum method. J. Mech. Phys. Solids. 47, 611-642.
Tadmor, E. B., Miller, R. E., 2007. Quasicontinuum method website. www.qcmethod.com.
Taupin, V., Varadhan, S., Chevy, J., Fressengeas, C., Beaudoin, A.J., Montagnat, M., Duval, P., 2007. Effects of size on the dynamics of dislocations in ice single crystals. To appear in Physical Review Letters.
Truesdell, C. A., Toupin, R. A. 1960. in Principles of Classical Mechanics and Field Theory, Encyclopedia of Physics, Vol. III/1, edited by S. Flügge, (Springer-Verlag, Berlin, Göttingen, Heidelberg), 226-790.
Tsai, D. H. 1979. The virial theorem and stress calculation in molecular dynamics J. Chem. Phys. 70 137582
van Vliet, K., Suresh, S., July 2002. Simulations of cyclic normal indentation of crystal surfaces using the bubble-raft model. Phil. Mag. A 82(10), 1993-2001.
van Vliet, K. J., Li, J., Zhu, T., Yip, S., Suresh, S., 2003. Quantifying the early stages of plasticity through nanoscale experiments and simulations. Phys. Rev. B 67, 104105.

Varadhan, S., Beaudoin, A.J., Fressengeas, C., 2005. Coupling the dynamics of statistically distributed and excess dislocations. Proceedings of Science, http://pos.sissa.it/archive/conference/023/004/SMPRI2005_004.pdf.

Varadhan, S., Beaudoin, A.J., Acharya, A., Fressengeas, C., 2006. Dislocation transport using and explicit galerkin/least-squares formulation. Modelling and Simulation in Materials Science and Engineering 14, 1245-1270.

Ziegenbein, A., Achmus, Ch., Plessing, J., Neuhäuser, H., 1995. On Lüders band formation and propagation in CuAl and CuMn single crystals. In Plastic and Fracture Instabilities in Materials, ASME AMD-Vol. 200/MD-Vol. 57, 101-119.

Zuev, L.B., 2007. On the waves of plastic flow localization in pure metals and alloys. Annalen der Physik 16, 286-310.